Surface & Coatings Technology 290 (2016) 124–134

Contents lists available at ScienceDirect

Surface & Coatings Technology

journal homepage: www.elsevier.com/locate/surfcoat

Comparison of structural, mechanical and corrosion properties of thin TiO_2/graphene hybrid systems formed on Ti–Al–V alloys in biomedical applications

M. Kalisz [a,*], M. Grobelny [a], M. Świniarski [b], M. Mazur [c], D. Wojcieszak [c], M. Zdrojek [b], J. Judek [b], J. Domaradzki [c], D. Kaczmarek [c]

[a] Motor Transport Institute, Centre for Material Testing, Jagiellonska 80, 03-301 Warsaw, Poland
[b] Faculty of Physics, Warsaw University of Technology, Koszykowa 75, 00-662 Warsaw, Poland
[c] Wroclaw University of Technology, Faculty of Microsystem Electronics and Photonics, Janiszewskiego 11/17, 50-372 Wroclaw, Poland

ARTICLE INFO

Article history:
Received 26 May 2015
Revised 5 August 2015
Accepted in revised form 7 August 2015
Available online 12 August 2015

Keywords:
Titanium dioxide thin film
Nanoindentation
Electrochemical properties
Graphene
Magnetron sputtering with modulated plasma

ABSTRACT

In this paper, comparative studies on the mechanical and corrosion properties of hybrid coating systems based on titanium dioxide thin films (200 nm) and graphene monolayers have been investigated. The pure titanium dioxide layers were deposited on a Ti6Al4V alloy surface using the conventional magnetron sputtering process and the so-called "magnetron sputtering with modulated plasma" process. A graphene monolayer was transferred to a titanium alloy substrate using the "PMMA-mediated" method. The structural characteristics of the obtained thin films were examined by using Raman spectroscopy, X-ray diffraction (XRD), a scanning electron microscope (SEM) and atomic force microscopy (AFM) measurement. The mechanical properties, i.e. hardness, were tested by using a nanoindenter test. The corrosion properties of the coatings were determined by analysis of the voltammetric curves.

The deposited TiO_2 thin film prepared by the conventional magnetron sputtering process consisted of visible grains with the size of ca. 50–100 nm and had a nanocrystalline anatase phase (TiO_2(a)). The TiO_2 thin film deposited by plasma-modulated sputtering had a nanocrystalline rutile structure TiO_2(r) and its surface consisted of big, irregular grains and was not as homogeneous as the coating prepared by the conventional method.

The hardness of TiO_2(a) and TiO_2(r) thin films was equal: 7.59 GPa and 14.2 GPa, respectively.

Graphene transferred to a titanium dioxide thin film surface was a single layer without defects. Unfortunately, the nanoindentation method, used to measure the hardness of the titanium dioxide/graphene coating systems, is not sensitive to one or few atomic layers of graphene deposited on the top of the coating structures. Therefore, the measurement did not reveal changes of titanium dioxide thin film hardness after graphene deposition, in comparison with uncoated TiO_2 thin films such as TiO_2(a) and TiO_2(r) thin films. Futhermore, the graphene monolayer can be very easily removed from the titanium dioxide thin film surface (e.g. by scratching).

The best corrosion properties (the lower value of corrosion current density) were obtained for sample Ti6Al4V coated with a TiO_2(a) thin film. A deposition graphene monolayer on the top of all tested thin films improves the corrosion potential (E_{corr}) value, which is much more positive than E_{corr} registered for the other samples. A positive value of the corrosion potential is characteristic of materials with low electrochemical activity and thereby very good corrosion resistance. Moreover, these coatings systems maintain stability of the mechanical properties during the corrosion process.

1. Introduction

Metallic biomaterials like Ti and Ti alloys are widely used in artificial hip joints, bone plates and dental implants due to their excellent mechanical properties and endurance [1]. However, the long-term performance of surgical implants is directly dependent on their surface properties. Most implanted metallic biomaterials have a tendency to lose electrons in solution and, as a result, they show a high potential to corrode in biological environments, which usually cause inflammations and loosening of the implants [2]. Corrosion is an unwanted chemical reaction, which can result in the degradation of metal implants to oxides, hydroxides, or other compounds. These degradation products may cause a local inflammatory response, leading to the cessation of bone formation, synovitis, and loosening of artificial joint implants [2]. Additionally, their low surface hardness, high friction coefficient and poor wear resistance also limit their application as metallic biomaterials [3,4]. Low wear resistance can lead to the formation of wear debris

* Corresponding author.
E-mail address: malgorzata.kalisz@its.waw.pl (M. Kalisz).

http://dx.doi.org/10.1016/j.surfcoat.2015.08.011
0257-8972/

which may cause several reactions in the tissue in which they are deposited, thus increasing the failure probability of the implants.

It has been reported that wear and corrosion are the main reasons for degradation of surgical implants such as hip and knee joint implants, which usually happens after 10–15 years of use [4]. To protect metallic implants from corrosion and wear and improve their bioactivity, tremendous surface modification techniques have been applied to deposit a great variety of functional coatings on the surfaces of metallic implants.

Usually, there are two ways to improve the corrosion and the wear resistance of a metal implant. One is via bulk alloying and the second is the use of surface modification. Since this paper only focuses on the surfaces of metal implants, the first technology is not covered here.

One way to protect a titanium alloy surface from corrosion and improve its surface mechanical properties is the application of ceramics coatings, i.e. titanium dioxide. Titanium oxide film is a very important material due to its multifunctional application in photocatalysis, hydrophobic material, photovoltaic cells, photochromic and electrochromic devices, gas sensors, biosensors, corrosion protection, bactericide and optical devices, among other things [5–8]. TiO_2 can occur in a number of crystalline forms, the most important of which are anatase, rutile and brokite. Nowadays, it is one of the most extensively studied metal oxides, both as a particulate and in thin film form. Titanium dioxide thin film properties depend on the crystalline phase, roughness, porosity, and particle size and distribution.

Unfortunately, the addition of a protective coating changes the dimensions of metals due to the finite thickness of the coating. Changes also occur in the appearance and the optical properties of the metal surface; furthermore, decreases in the electrical and thermal conductivity can also be observed. One important approach to overcoming these problems would be to develop an ultrathin protective coating to minimize the variation in physical properties of the protected metal.

Graphene is a monolayer of carbon atoms, with a near-perfect two-dimensional honeycomb crystal lattice. This material has many useful electrochemical characteristics, and with its high thermal conductivity, high inherent capacity and extremely large specific surface area, graphene outperforms many other materials. Numerous studies have demonstrated that graphene film, which features chemical inertness and thermal stability, is an excellent anticorrosion barrier for Cu [9–14] and others metals like Ti [15].

It is reasonable to combine both types of materials in a hybrid coating system having a thickness of several hundred nanometers, characterized by good mechanical properties and excellent corrosion resistance in aggressive environments, e.g. body fluids.

In this work we show that hybrid coating systems based on titanium dioxide thin films (200 nm) and a graphene monolayer can be used as a protection system for a titanium alloy surface against the corrosion process and to improve its surface mechanical properties. To show this, we study surface, structural, mechanical and corrosion properties of two coating systems i.e. Ti–Al–V/TiO_2 and Ti–Al–V/TiO_2/graphene, and compare them with a pure titanium alloy.

2. Materials and methods

2.1. Experimental design

2.1.1. Specimen preparation

For the purpose of the experiment, four sets of titanium alloy Ti6Al4V (ASTM Grade 5, UNS R56400) (Table 1) were prepared in the same manner. Before technological processes, the Ti alloy surfaces were polished using a grinding and polishing Stuers RotoPol 21 apparatus. The sample surfaces were polished to a "mirror image". In the next stage, the samples were cleaned in an acetone solution.

Table 1
Composition of Ti6Al4V titanium alloy.

Components, wt.%						
C	Fe	N	O	Al	V	Ti
0.08	0.25	0.05	0.20	5.50–6.75	3.5–4.5	Bal

2.1.2. Thin film preparation

2.1.2.1. Ti–Al–V/titanium dioxide system preparation. For the deposition of thin films, a home-invented multitargeted apparatus for magnetron sputtering with an innovative system of target power control was used. The control system of this apparatus is protected by a patent application [16]. Each magnetron is independently powered by its individual supplier (DORA Power Systems), controlled by a microprocessor controller. The sputtering workstation is equipped with a standard vacuum chamber, a pump system (diffusion and rotary pumps), four magnetrons, a stage with the possibility of motion in the XYZ directions, Pfeiffer vacuum gauges and a gas flow control system that involves MAKS mass-flow controllers. Two sets of titanium dioxide thin films were deposited using conventional and so-called "magnetron sputtering with modulated plasma". TiO_2 thin films were deposited on silicon (100), fused silica (SiO_2) and titanium alloy Ti6Al4V substrates by reactive magnetron sputtering process from a pure metallic titanium target. Thin films deposited on silicon and SiO_2 were used to evaluate the surface morphology and structural properties, respectively. Coatings prepared on Ti6Al4V substrates were used to determine mechanical and electrochemical properties. In the conventional process, a continuous flow of oxygen was preserved at 40 ml/min. Oxygen was used both as a working and a reactive gas. During the sputtering process the pressure in the vacuum chamber was kept at ca. $2 \cdot 10^{-2}$ mbar. The time of thin film deposition was equal to 120 min. In the process with modulated plasma, oxygen was also used as a working and a reactive gas. The time of sputtering was twice as long as in the case of the conventional process. Moreover, the pressure during deposition was significantly lower and equal to ca. $2 \cdot 10^{-3}$ mbar. The innovation in this process was the introduction of oxygen into the vacuum chamber in short (few tens of milliseconds) pulses, controlled by a special gas injection system.

2.1.2.2. Ti–Al–V/TiO_2/graphene system preparation. The graphene monolayers were grown on 18-μm thick copper foil using the chemical vapor deposition (CVD) technique. For this purpose, a home-made CVD set based on a Blue M Tube Furnace with a 1-inch diameter reactor tube was used. During the growth process, the reactor chamber is set at low pressure (~10^{-6} Torr) and heated up to ~1000 °C in a hydrogen atmosphere. Methane is used as a carbon source (growth time is typically 10 min).

Graphene was transferred to titanium dioxide thin films using a "PMA-mediated" method [18]. First, PMA (495 K, about 100 nm thick) was spin-coated on top of the synthesized graphene on copper substrate and dried for 24 h at room temperature. Next, the graphene from the bottom of the Cu substrate was etched using the reactive ion etching method in oxygen plasma (Plasma Lab 80+, Oxford Instruments). After that, the exposed Cu foil was dissolved in an aqueous etchant of iron (III) nitrate for several hours. When the copper was dissolved, the graphene sample was cleaned in DI (deionized) water. Next, an ion particle removing step was used with a hydrochloric acid solution, with hydrogen peroxide as a catalyst dissolved in water [18]. After all the cleaning steps, a PMA/graphene layer was transferred to a titanium dioxide surface and annealed in order to evaporate the water and increase adhesion between the graphene and the surface. In the last step, the PMA layer was removed.

2.2. Analysis of surface characteristics

Structural properties of TiO_2 thin films were determined based on the results of the X-ray diffraction (XRD). For the measurements, a

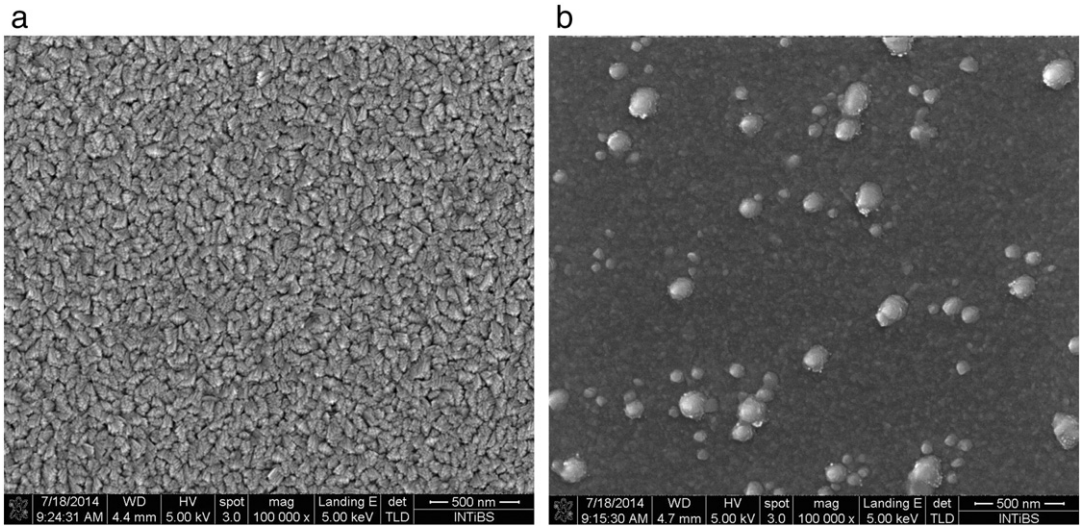

Fig. 1. SEM images of the surface of TiO_2 thin films deposited by: a) conventional and b) plasma modulated magnetron sputtering processes.

Siemens 5005 powder diffractometer with a Co K X-ray (1.78897 Å) was used. The correction for the broadening of the XRD instrument was accounted for and the crystallite sizes were calculated using Scherer's equation [17].

The thickness of deposited titanium dioxide thin film was measured by Taylor Hobson Tal surf CCI Late optical profilometry and was equal to 200 nm.

The quality and number of transferred layers of graphene were evaluated by Raman spectroscopy (India Renishaw Spectrometer, 514 nm laser line, standard and streamline mode). All Raman spectra were collected at room temperature using <1 mW of laser power (on the sample).

Raman spectroscopy is a nondestructive and fast method for studying, e.g. various carbon materials. In the case of graphene, Raman spectra gives information about the number of layers [19], material quality and defects [20]. Typical Raman spectra consist of 3 main modes: D mode (~1350 cm^{-1}), G mode (~1580 cm^{-1}) and 2D mode (~2700 cm^{-1}). A monolayer graphene sheet is easily identified by Raman study simply by looking at the G/2D relative intensity ratio (usually about 0.2), also taking into account the shape of those peaks [19]. The quality and defectiveness of a graphene sheet can be verified by the appearance of the D mode peak, usually taken as the relative ID/IG ratio [21,22].

The elemental composition and the surface morphology of the coating were investigated with the aid of a FESEM FEI Nova NanoSEM 230 scanning electron microscope (SEM). The SEM images were obtained using a Low Voltage High Contrast vCD Detector, which is effective for low voltage (<3 kV) backscattered electron imaging.

To determine the surface topography properties, atomic force microscopy (AFM) measurements were made with a UHV VT AFM/STM Omicron (Oxford Instruments, Germany) microscope operating in ultra-high vacuum conditions in contact mode.

2.3. Mechanical characterization

The hardness measurements of the obtained coating system before and after the corrosion process was measured using the CSM Instrument, Peseux, Switzerland nanoindenter equipped with Vickers diamond indenter. The hardness was calculated using the method proposed by Oliver and Pharr [23] with Poisson ratio of 0.3. Each data point represents an average of five indentations.

To determine the mechanical properties of thin films by nanoindentation, it is important to recognize the influence of the substrate on measurement results. The "10% principle" is commonly used to minimize the substrate impact — the nanoindentation depth should be less than 10% of the measured layer thickness [24]. In our case, this principle cannot be applied to layers which have a thickness of about 200 nm, as it would require a nanoindentation depth of less than 20 nm. However, meaningful results at such low indentation depths are not possible with the current state of indentation equipment. This is mainly due to the inability to define a correct and applicable area function for the indentation tip at very shallow penetration depths [25]. In our case, experiments have shown that the tip area function is not a significant source of error for indentations of contact depths larger than about 80 nm [26]. Unfortunately, for this indentation depth, the influence of the substrate on the measurement results is too big. Therefore, it is necessary to develop and apply different methods of analysis, interpretation and approximation of results in order to obtain real values of hardness and Young modulus of thin films deposited on a substrate. Many mathematical models have been developed allowing investigation

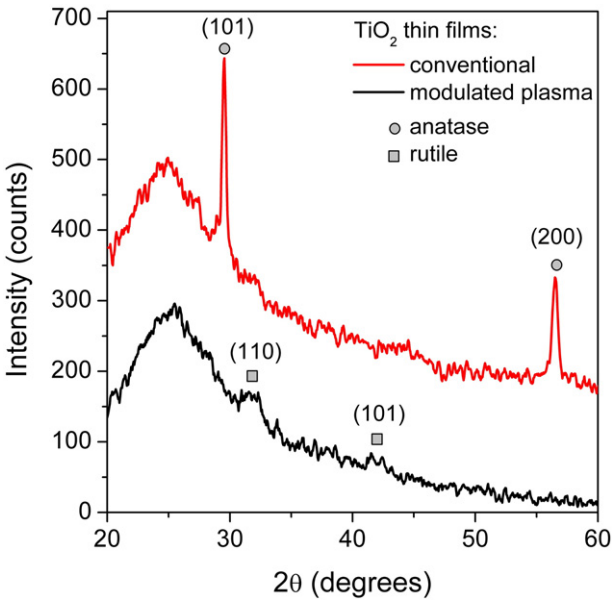

Fig. 2. XRD measurement results of TiO_2 deposited by conventional and with modulated plasma magnetron sputtering processes [18,19].

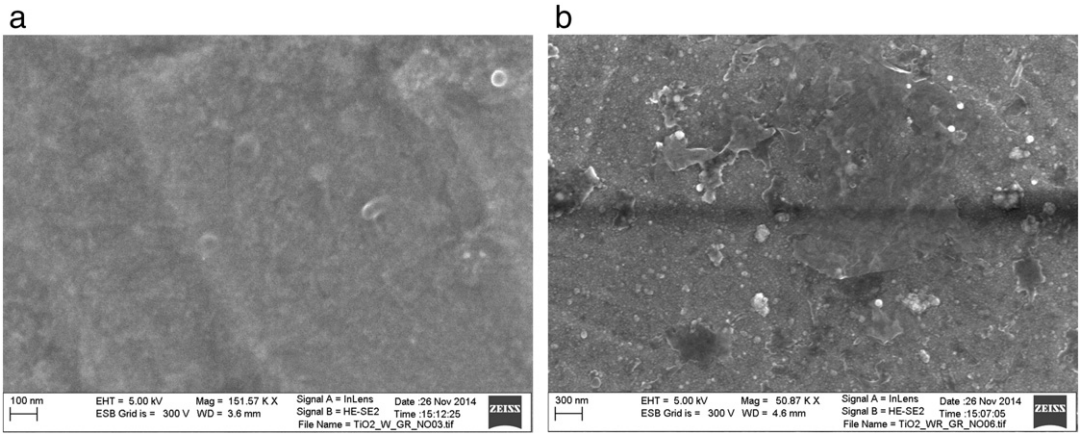

Fig. 3. SEM images of the surface of a) deposited TiO_2(a)/graphene coating system before corrosion process, b) deposited TiO_2(r)/graphene coating system before corrosion process.

and approximation of the measurement values [27–30] of thin films. In our research we used the approximation methods described in article [25]. If the properties of the substrate (i.e. hardness) and the thickness of the film are known, a series of measurements of the hardness for many indentation depths (to the extent that the measurement error is negligible) can be performed, and it is possible to determine the approximate parameters of the layer without affecting the substrate.

The measured hardness of the layer/substrate structure can be expressed as a power-law function of the substrate and thin film hardness, the depth of indentation and the thickness of the thin film [25]:

$$H = H_s \times \left(H_f / H_s\right)^M \tag{1}$$

where H_s is the hardness of the substrate, H_f the hardness of the thin film and M the dimensionless spatial function defined by [25]:

$$M = 1/\left(1 + K(h/d)^L\right) \tag{2}$$

where K, L are adjustable coefficients, h is the maximum indenter displacement and d is the thickness of the thin film. Eq. (1) must satisfy essential boundary conditions: when indentation depth approaches zero: $h/d \to 0$, $H = H_f$, $L = 1$ and $M = 1$ (small penetrations), the measured value of hardness tends to the value of hardness of the thin film, whereas when indentation depth approaches thin film thickness: $h/d \to \infty$, $H = H_s$, $L = 0$ and $M = 0$ (large penetrations), the measured value of hardness tends to the value of hardness of the substrate.

2.4. Electrochemical measurements

Electrochemical measurements were carried out in 0.5 M/l NaCl, 2 g/l KF, pH = 2 adjusted by concentrated hydrochloric acid. The solution (0.5 M NaCl, pH 2, 2 g/l KF) in which the electrochemical measurements were conducted is characterized by high corrosivity compared to titanium alloys. It is a more aggressive environment than that of typical electrolytes for corrosion tests (e.g. artificial saliva, SBF). Voltammetric measurements (polarization curves) were carried out at a scan rate of 1 mV/s within the range of −150 mV to 1000 mV versus open circuit potentials, and polarization curves corresponding to all examined material were recorded. Prior to each polarization experiment, the samples were immersed in the electrolyte for 1 h while monitoring open circuit potential to establish steady state conditions. Each electrochemical measurement for the same material was performed three times. In the paper we show only the most representative results. However, the differences between the successive values of the open circuit potential (for the same material) did not exceed 50 mV. A three-electrode cell arrangement was applied using the Ag/AgCl electrode with a Luggin capillary as the reference electrode and a platinum wire as the auxiliary electrode (counter-electrode). The measurements were carried out by means of an Autolab EcoChemie System of the AUTOLAB PGSTAT 302N type equipped with GPESv. 4.9 software in aerated solutions at room temperature. The

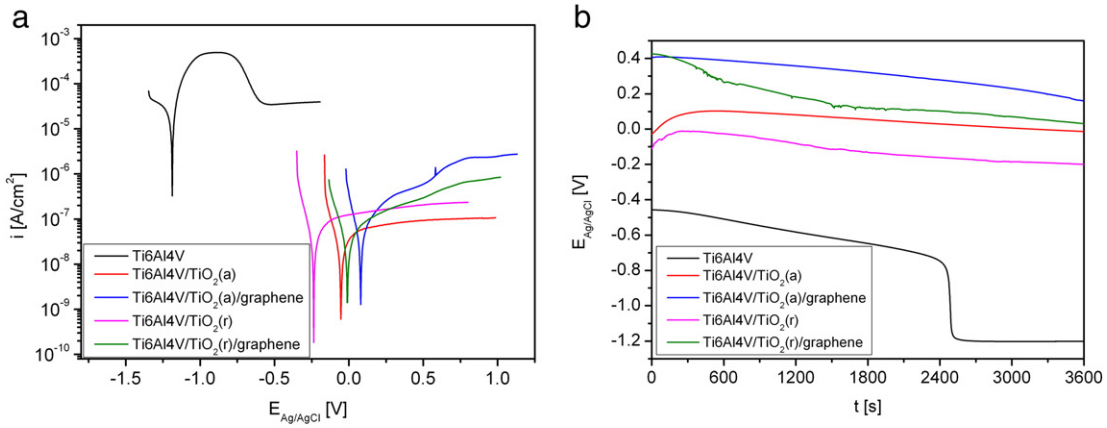

Fig. 4. Open circuit potential (OCP) (a) and polarization curves (b) of Ti6Al4V titanium alloy and titanium alloy with coating system.

Table 2
Electrochemical parameters of the samples obtained from polarization curves in 0.5 M/l NaCl, 2 g/l KF, pH = 2 electrolyte solution.

Sample	i_{corr} [A/cm^2]	E_{corr} [V]
Ti6Al4V/TiO_2(a)	2.6E−08	−0.054
Ti6Al4V/TiO_2(a)/graphene	6.5E−08	0.079
Ti6Al4V/TiO_2(r)	5.4E−08	−0.237
Ti6Al4V/TiO_2(r)/graphene	4.2E−08	−0.010

values of corrosion current densities (i_{corr}) were obtained from the polarization curves by extrapolation of the cathodic and anodic branch of the polarization curves to the corrosion potential [31].

3. Results and discussion

3.1. Structural characterization of Ti–Al–V/TiO_2 and Ti–Al–V/TiO_2/graphene hybrid systems before corrosion process

The results of SEM investigations (before the corrosion process) revealed that the surface of thin films prepared by the conventional magnetron sputtering process consisted of visible grains (Fig. 1a). However, obtained SEM images of the TiO_2 deposited by plasma-modulated sputtering showed that the thin film surface was not as homogeneous as for the coating prepared via the conventional method and consisted of large, irregular grains (Fig. 1b).

XRD measurement results (Fig. 2) showed that titania thin films deposited by the conventional magnetron sputtering process had a nanocrystalline anatase phase with a crystallite size of approximately 27.3 nm. The diffraction peaks were intense, indicating that these coatings were well crystallized. In the case of TiO_2 thin films deposited by magnetron sputtering with modulated plasma, analysis of diffraction patterns resulted in the appearance of some small trace amounts of fine crystallites with a rutile phase. However, the peak related to the (110) plane at ca. 32° (2θ) was broad and had very low intensity. Therefore, taking into consideration that the signal-to-noise ratio (S/N) was rather poor, the determination of crystallite dimensions could be encumbered with an error. At the sensitivity level of the XRD method, it can be assumed that these coatings were nanocrystalline and consisted of small rutile crystallites with a size of ca. 5.8 nm. Such broadening of the XRD pattern can also indicate that a large amount of amorphous phase occurred in these coatings. Additionally, the broadening of the intensity of the XRD pattern at 20–30° (2θ) is related to the amorphous fused silica substrate on which both TiO_2 thin films were deposited.

Titanium dioxide thin films were deposited using various modifications of the magnetron sputtering method: with the continuous working gas flow, herein called “conventional sputtering”, and with plasma modulated by supplying the working gas in pulses. The idea applied in sputtering with modulated plasma was similar to what is described in the literature as gas injection magnetron sputtering (GIMS) [32].

Various morphologies and especially microstructures can be related to the pressure during the deposition process. In the case of conventional sputtering with a continuous gas flow, the pressure was kept at the level of $2 \cdot 10^{-2}$ mbar. In the case of the process with modulated plasma, the working gas (pure oxygen) was injected directly into the target surface in short (few tens of milliseconds) pulses. Therefore the pressure during sputtering could be maintained at the level of an order lower (about $2 \cdot 10^{-3}$ mbar) than in conventional deposition. Such a change led to an increase of the particles' mean free path and resulted in higher energy of the particles that reached the substrate. Therefore, the lower pressure during sputtering was responsible for obtaining the TiO_2 rutile phase directly after deposition using the plasma modulated process instead of anatase in the conventional one.

For the purposes of this article, a titanium dioxide thin film of anatase structure will be denoted TiO_2(a) and of rutile structure — TiO_2(r).

In Fig. 3, SEM images of the surface of the TiO_2 thin films after graphene monolayer deposition are shown. The investigated titanium dioxide/graphene hybrid systems were crack- and damage-free, no discontinuity in the coating systems was observed, and the surface morphology was homogeneous.

3.2. Potentiodynamic tests

Fig. 4 shows the course of the open cell potential (OCP) (Fig. 4b) and the course of polarization curves of titanium alloy and titanium alloys with coating systems (Fig. 4a) in a 0.5 M/l NaCl, 2 g/l KF, pH = 2 electrolyte solution. The results of measurements of the electrochemical parameters of the samples obtained from polarization curves are collected in Table 2.

In the case of the titanium alloy with coatings, a significant improvement in the corrosion properties is seen, expressed by a decrease of the corrosion current density i_{corr} and a shift of the corrosion potential E_{corr} values to the noble potentials.

The smallest corrosion current density and the best corrosion properties were obtained for the Ti6Al4V/TiO_2(a) coating system. However, the corrosion potential value for the TiAlV/TiO_2(a)/graphene coating system was E_{corr} = 0.079 V, which is much more positive than E_{corr} registered for the other samples. A positive value of the corrosion potential is characteristic of materials with low electrochemical activity and thereby very good corrosion resistance.

It should also be noted that the course of the potential for all examined samples is very stable. During a 1-hour exposure, the potential changed only by about 80 mV for a Ti6Al4V/TiO_2(a) sample, 180 mV

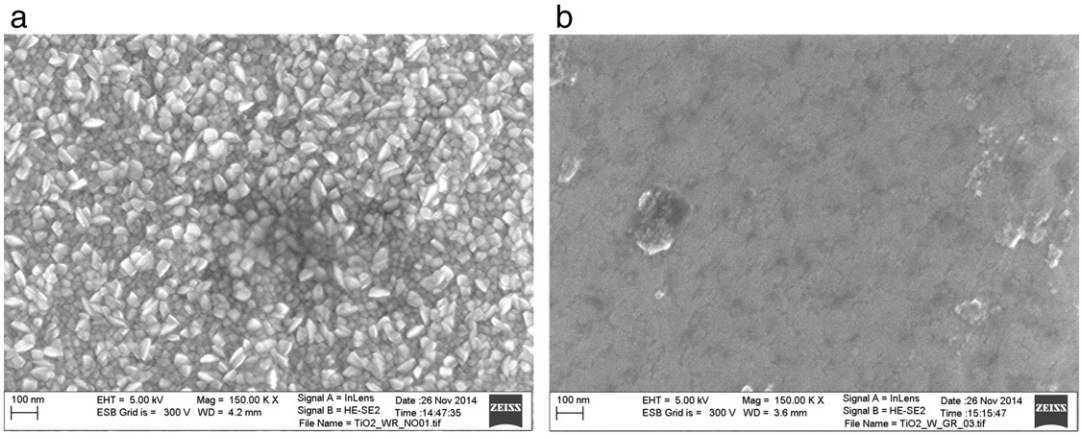

Fig. 5. SEM images of the surface of TiO_2 thin films deposited by: a) conventional and b) plasma modulated magnetron sputtering processes, after corrosion process.

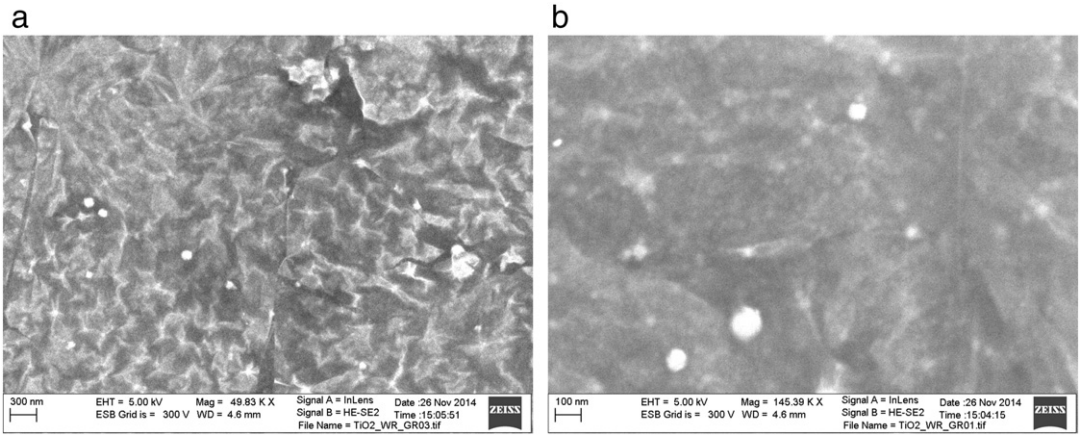

Fig. 6. SEM images of the surface of a) deposited TiO_2(a)/graphene coating system after corrosion process, b) deposited TiO_2(r)/graphene coating system after corrosion process.

for a Ti6Al4V/TiO_2(r) sample, 240 mV for a Ti6Al4V/TiO_2(a)/graphene sample, and 400 mV for a Ti6Al4V/TiO_2(r)/graphene sample.

For the uncoated titanium alloy sample, a sharp decline in the value of the potential from −0.75 V to −1.20 V takes place. However, this change is caused by damage of the oxide layer present on the surface of a titanium alloy. The oxide layer acts as a barrier and protection against general corrosion processes. However, in the environment of acidic pH (pH ca. 2) the protective layer is unstable and the processes of corrosion of metallic Ti or its alloys are initiated. This phenomenon is accelerated in the presence of aggressive ions such as fluoride ions [33–36].

The results obtained indicate that the titanium dioxide films and titanium dioxide/graphene coating systems formed on the titanium alloy surface can inhibit the aggressive action of corrosion media [37].

3.3. Structural characterization of Ti–Al–V/TiO_2 and Ti–Al–V/TiO_2/graphene hybrid systems after corrosion process

The surface morphology of the titanium dioxide films after corrosion testing was studied by SEM. No clear and large corrosion pit was found on the surfaces of the titanium dioxide films [37]. The surface of the tested thin films was smooth and compact. This confirms the results obtained from the corrosion tests, described above (Fig. 5).

Deposition of the graphene monolayer on top of the titanium dioxide thin films causes the formation of dendritic structures on the surface of the coating systems after the corrosion tests (see Fig. 6).

In Fig. 7 the AFM image for titanium dioxide/graphene coating systems is shown. It is clearly seen that after the corrosion process, the regions in the gaps changed color (white), indicating that those regions formed an oxide layer [38]. On the microscopic scale, the graphene layer transferred to the top of the titanium dioxide layer is not a single sheet of carbon atoms, but many small single-layer graphene sheets connected together. The most likely breakdown location is along the graphene grain boundary (along the places where graphene sheets connect together). The graphene grain mismatch along the grain boundary is a likely target for oxygen molecules to sneak in and oxidize the thin film located below. The white spots in AFM images are the places that allow oxygen molecules to sneak in and oxidize the surface of the titanium dioxygen thin film located below the graphene. These white spots have a height ranging from 90 nm to 180 nm, depending on the type of TiO_2 layer [39]. The places located below the graphene monolayer grain boundaries are oxidized, resulting in the AFM images' white spots, more or less branched on two or three sides (see Fig. 7). In the SEM images, these oxidized regions can be interpreted as dendritic structures. The shape and distribution of dendrites is different for both coating systems, probably because of differences in the original

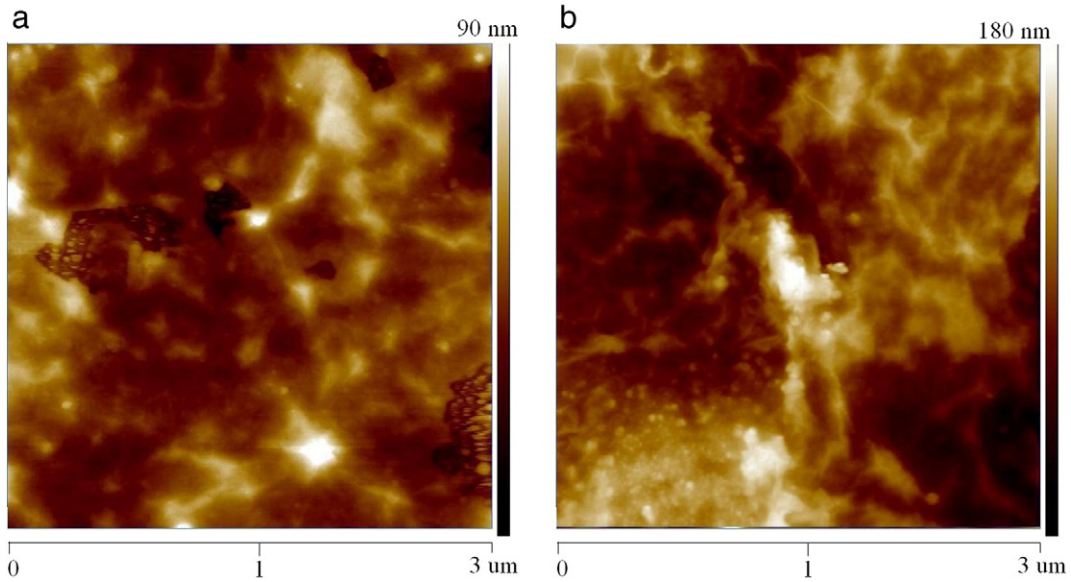

Fig. 7. AFM image of a) deposited TiO_2(a)/graphene coating system after corrosion process, b) deposited TiO_2(r)/graphene coating system after corrosion process.

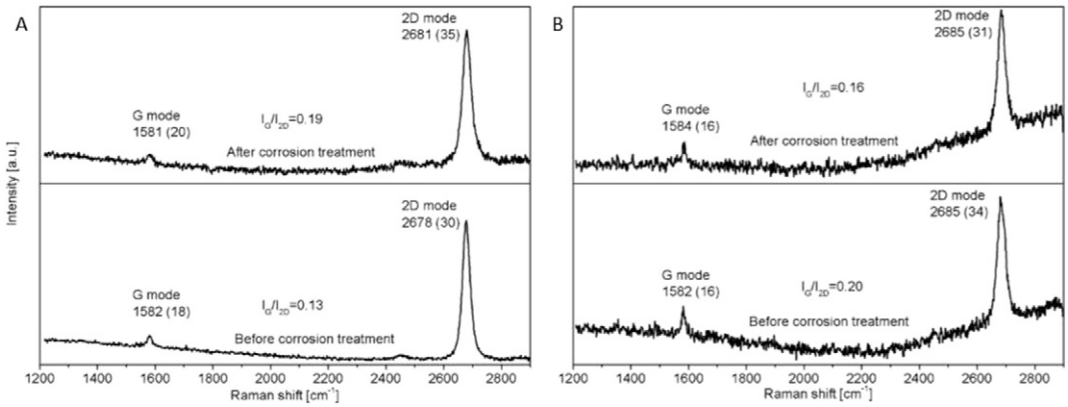

Fig. 8. Comparison of Raman spectra before and after corrosion measurements for both samples: (A) TiAlV/TiO_2(a)/graphene and (B) TiAlV/TiO_2(r)/graphene. All spectra were collected using the same measurement parameters (514 nm laser line, 45 s of exposure time and two accumulations).

structure of the obtained titanium dioxide thin films. The titanium dioxide regions under the graphene flakes are pristine, which indicates that these regions are not oxidized [38]. The titanium dioxide regions located under the graphene flakes are better protected than regions located under the gaps. The surfaces of titanium dioxide/graphene coatings systems are still densely packed after the corrosion process.

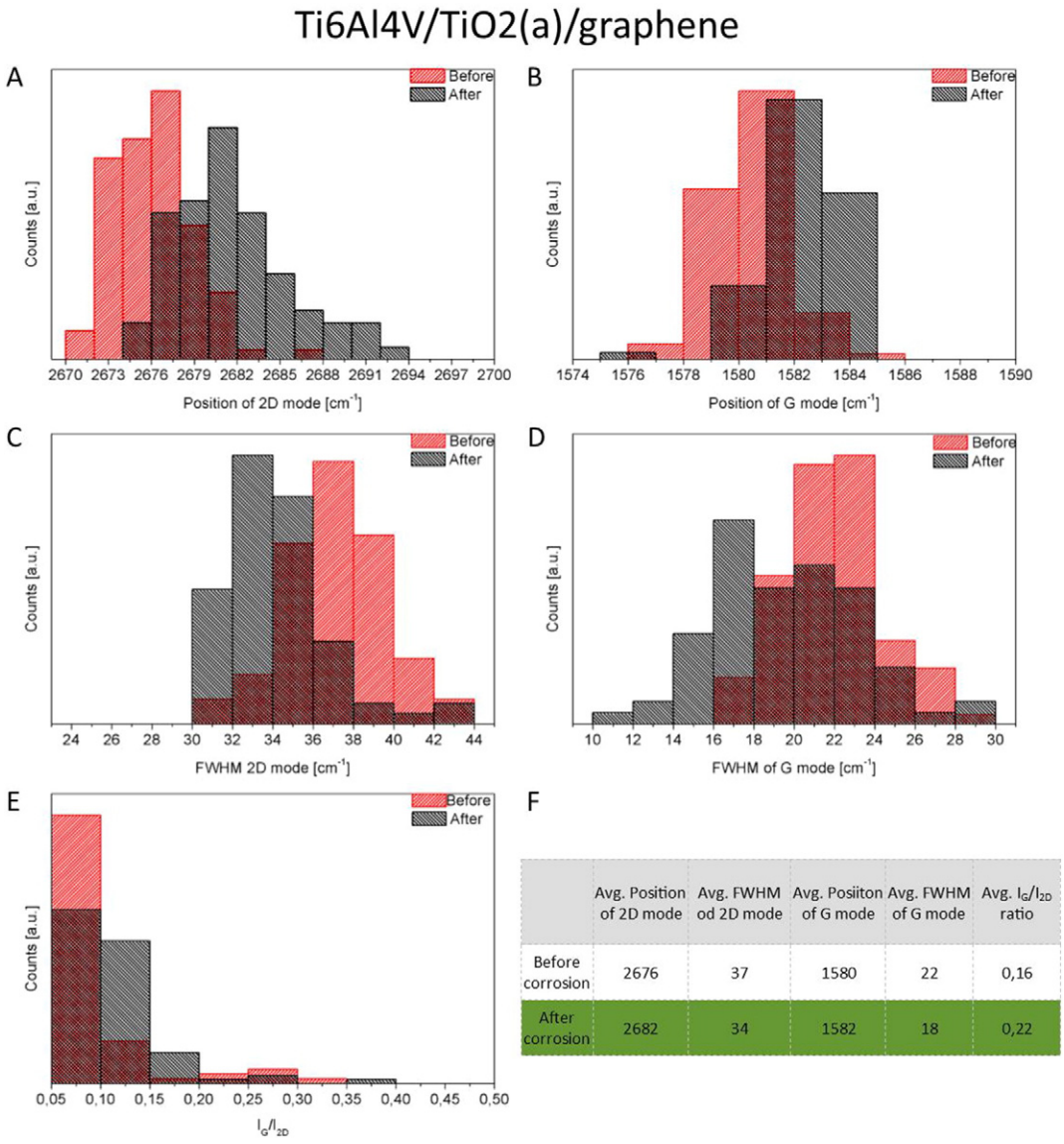

	Avg. Position of 2D mode	Avg. FWHM od 2D mode	Avg. Posiiton of G mode	Avg. FWHM of G mode	Avg. I_G/I_{2D} ratio
Before corrosion	2676	37	1580	22	0,16
After corrosion	2682	34	1582	18	0,22

Fig. 9. Histograms showing spatially resolved characteristic parameters of Raman spectra (G and 2D peak position and FWHM, I_G/I_{2D} intensity ratio) for sample Ti6Al4V/TiO_2(a)/graphene. Parameters were collected using Raman mapping mode where 10 × 10 μm with 2 μm step map was done.

3.4. Raman characterization of graphene layer in Ti–Al–V/TiO_2/graphene hybrid systems

Raman spectra were collected for both samples with the same measurement parameters.

Fig. 8 shows Raman spectra collected before and after corrosion measurements for both samples with titanium dioxide/graphene layers. In both cases, the absence of the D mode indicates that the graphene layer is continuous without structural defects [20–22]. We note that the signal of the D band has been recorded in many spots on the samples, showing no significant difference from place to place. For a sample with a rutile structure of TiO_2 (Fig. 1(A)), the intensities of graphene representative modes are two times smaller (intensity count not shown in figure) than in the case of the anatase phase of TiO_2, which can be caused by a different surface effect (different surface adhesion of graphene to the oxide layer) [40]. In the case of the second sample (structure of anatase), the intensities are quite similar before and after corrosion. For a better understanding of what happened after corrosion treatment with a carbon sheet, we made Raman maps (~100 spectra from the selected area) for both samples, in both areas (before and after corrosion treatment).

The statistics show peak position shifts in both G (~2 cm^{-1}) and 2D modes (~6 cm^{-1}). The shifting of those two modes (Fig. 9A, B) can be caused by doping of the graphene layer during the chemical transfer process. Chemical transfer could leave Fe^{3+} ions after copper etching or some PMMA residues after dissolving in acetone.

For the second sample (Ti6Al4V/TiO_2(r)/graphene), see Fig. 10; the differences between collected results in both areas are smaller than for the rutile sample. In the case of the positions of the 2D mode, after the corrosion process there is a little upshift (~2 cm^{-1}). Smaller shifts and intensities of graphene representative modes in the rutile sample can be caused by similar adhesion to the surface in both areas (before and after corrosion) and by less contamination of the second sample.

The relative intensity ratios in both samples indicate that the measured area is covered by a single layer of graphene [21,22]. The mapped areas exhibit the absence of the D mode, which confirms the continuity of the transferred layer from copper. Moreover, the fact that no D mode

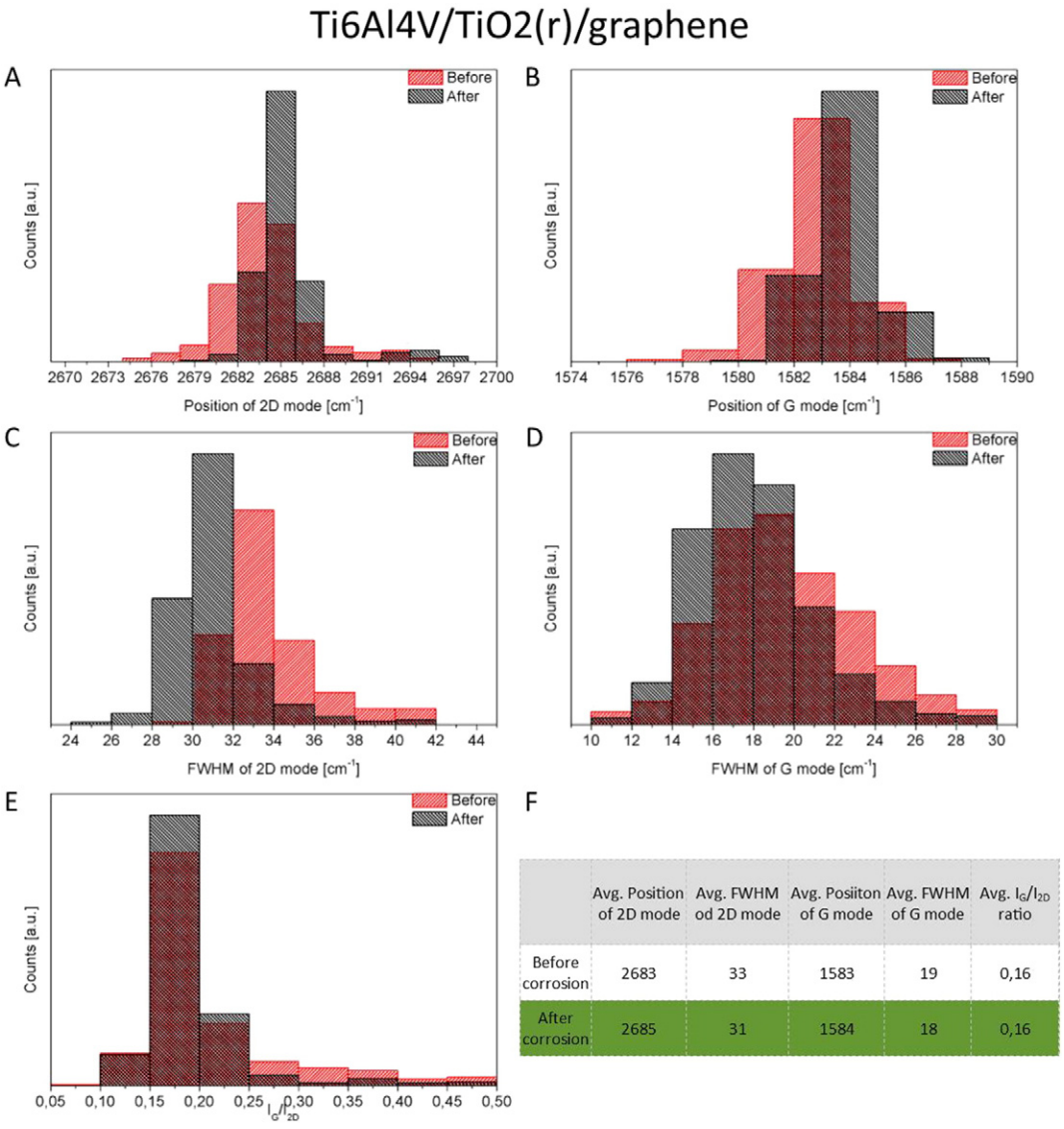

	Avg. Position of 2D mode	Avg. FWHM od 2D mode	Avg. Posiiton of G mode	Avg. FWHM of G mode	Avg. I_G/I_{2D} ratio
Before corrosion	2683	33	1583	19	0,16
After corrosion	2685	31	1584	18	0,16

Fig. 10. Histograms showing spatially resolved characteristic parameters of Raman spectra (G and 2D peak position and FWHM, I_G/I_{2D} intensity ratio) for sample. Ti6Al4V/TiO_2(r)/graphene. Parameters were collected using Raman mapping mode where 10 × 10 μm with 2 μm step map was done.

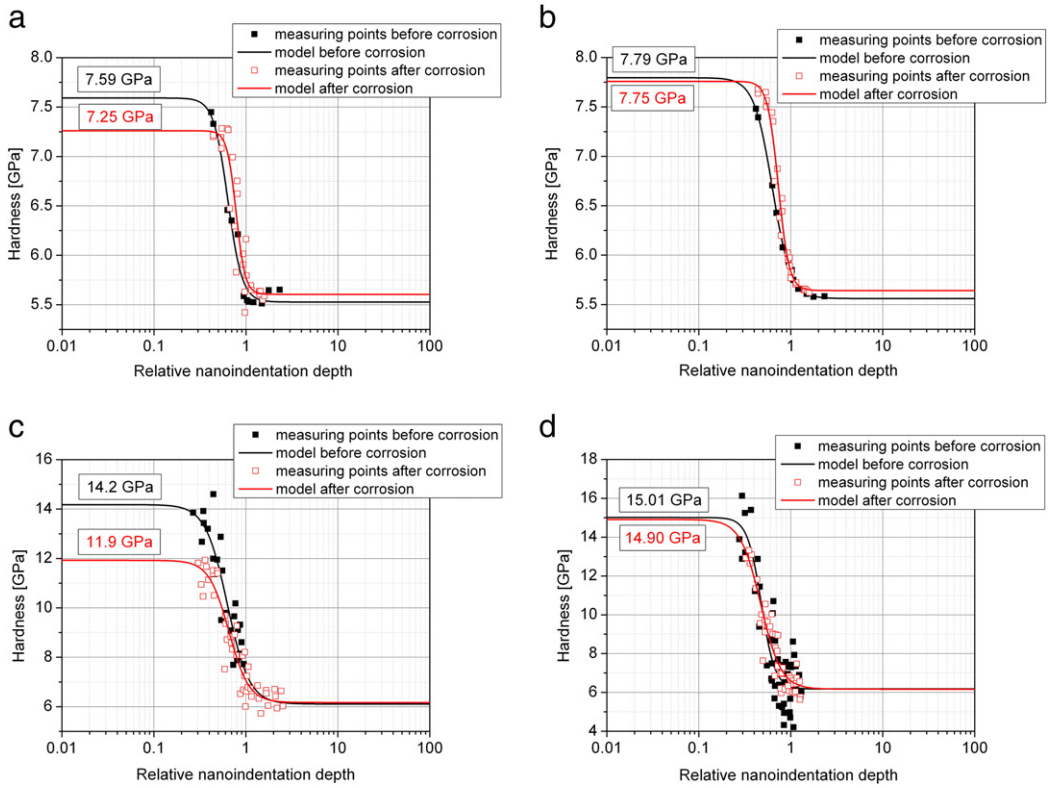

Fig. 11. Results of hardness investigation for a) TiO_2 (a) thin film, b) TiO_2 (a)/graphene coating system, c) TiO_2(r) thin film and d) TiO_2(r)/graphene coatings system, before and after corrosion process.

is seen after corrosion confirms the corrosion resistance property of a one-atom-thick carbon layer.

3.5. Mechanical characterization of prepared hybrid systems before and after corrosion process

The hardness of prepared coating systems was measured by nanoindentation and determined by an approximation method. For the uncoated titanium alloy, hardness has been measured at a constant depth of 80 nm, and was equal to 5.9 ± 0.3 GPa. The hardness of the titanium dioxide thin films deposited on clean titanium alloy substrates, with maximum indentation depth varying from 80 nm to 2000 nm, was measured. Additionally, the root mean square error (RMSE) was calculated.

Fig. 11 shows the measurements of the TiO_2 thin films and TiO_2/graphene coating system hardness (marked as points), whereas solid curves throughout the data points represent simultaneous regression best fits of Eqs. (1) and (2) to each data set. Yielding common coefficients are given in Table 3. Through measurements for a wide range of indentation depth, it was possible to determine the hardness of TiO_2(a) thin film, TiO_2(r) thin film, TiO_2(a)/graphene coating system and TiO_2(r)/graphene coating systems, which was equal at about: 7.59 ± 0.15 GPa (Fig. 11a), 14.2 ± 0.9 GPa (Fig. 11c), 7.79 ± 0.5 GPa (Fig. 11b) and 15.0 ± 0.8 GPa (Fig. 11d), respectively, without the influence of the titanium alloy substrate. As the obtained results show, the titania with a columnar rutile structure – TiO_2(r), deposited by the high-energy reactive magnetron sputtering process – had a hardness of 14–15 GPa, i.e. ca. 50% higher value compared to TiO_2 reported in the literature [41–46]. In contrast, the hardness obtained for titania with an anatase structure – TiO_2(a) – was 7.5 GPa, i.e. ca. 40% lower value compared to TiO_2 reported in the literature [47–54]. The TiO_2(r) film has a higher H value compared to TiO_2(a) as a result of a higher rutile content, which is consistent with previous experiments [50,52].

Our results show that the graphene monolayer deposited on titanium dioxide thin films is practically not seen by a nanoindenter during measurements. The nanoindentation method, used to measure the hardness of the titanium dioxide/graphene coating systems, is not sensitive to one or few atomic layers of graphene deposited on the top of the coating structures. Therefore, the measurement did not reveal changes of titanium dioxide thin film hardness after graphene deposition, in comparison with uncoated TiO_2 thin films such as TiO_2(a) and TiO_2(r) thin films.

Nanoindentation measurements performed after the corrosion process show no change of surface hardness for the tested samples coated by the TiO_2/graphene coating systems. For the TiO_2(a)/graphene coating system, hardness was equal to 7.75 ± 0.3 GPa and for the TiO_2(r)/

Table 3
Mechanical properties of titanium dioxide thin film and titanium dioxide/graphene coating systems.

Sample	Hardness before corrosion process [GPa]	*K*	*L*	Hardness after corrosion process [GPa]	*K*	*L*
Ti6Al4V/TiO_2(a)	7.59	10.7	5.56	7.25	7.56	8.68
Ti6Al4V/TiO_2 (a)/graphene	14.2	3.47	3.59	11.9	4.38	4.18
Ti6Al4V/TiO_2(r)	7.79	6.15	4.32	7.75	8.40	7.34
Ti6Al4V/TiO_2(r)/graphene	15.0	44.2	5.71	14.9	40.1	6.38

graphene coating system 14.9 ± 0.7 GPa. Only for uncoated titanium dioxide thin films was a slight decrease in hardness observed, from 7.59 ± 0.15 GPa to 7.25 ± 0.13 GPa for TiO_2(a) thin film and from 14.2 ± 0.9 GPa to 11.9 ± 0.7 GPa for TiO_2(r) thin film. The obtained results confirmed the results obtained from the corrosion test and structural measurements.

4. Summary

We have shown that TiO_2 thin films and TiO_2/graphene coating systems deposited on a titanium alloy surface can be considered to be barrier coating systems for a Ti6Al4V alloy. They protect its surface against corrosion processes which take place on a pure titanium alloy surface in very aggressive environments.

Out of all four tested coating systems, only the TiAlV/TiO_2(r) coating system can be considered to be a coating that improves the surface hardness of a Ti6Al4V alloy, from 5.9 GPa for an uncoated titanium alloy to 14.2 GPa for a titanium alloy covered by a thin TiO_2(r) film.

The deposition graphene monolayer on the top of all the tested thin films improves the corrosion potential value, which is much more positive than the E_{corr} registered for the other samples. A positive value of the corrosion potential is characteristic for materials with low electrochemical activity and thereby very good corrosion resistance. Moreover, these coating systems maintain stability of the mechanical properties during the corrosion process.

In the next step, investigations of the resistance to corrosion and the mechanical properties of hybrid systems during temporary exposure to corrosive environments (artificial saliva, SBF etc.) will be performed.

Acknowledgments

This work was financed by the National Centre for Research and Development for the years 2013–2016 as research project no. GRAF-TECH/NCBR/14/26/2013 “InGrafTi”.

This work was financed from the sources granted by the NCN as a research project number DEC-2013/09/B/ST8/00140 for the years 2014–2017 and DEC-2012/07/B/ST8/03760 in the years 2013–2016.

The authors would also like to acknowledge the financial support from Ministry of Science and Higher Education within the Juventus Plus program (no. IP2014 029473) for the years 2015–2017.

References

[1] M. Niinomi, Metallic biomaterials, J. Artif. Organs 11 (2008) 105–110.
[2] S.P. Patterson, R.H. Daffner, R.A. Gallo, Electrochemical corrosion of metal implants, AJR Am. J. Roentgenol. 184 (2005) 1219–1222.
[3] E. Ingham, J. Fisher, Biological reaction to wear debris in total joint replacement, Proc. Inst. Mech. Eng. H 214 (2000) 21–37.
[4] M. Spector, Biomaterial failure, Orthop. Clin. N. Am. 23 (1992) 211–217.
[5] F.L. Toma, G. Bertrand, S.O. Chwa, C. Meunier, D. Klein, C. Coddet, Comparative study of photocatalytic decomposition of nitrogen oxide using TiO_2 coatings prepared by plasma spraying and suspension plasma spraying, Surf. Coat. Technol. 200 (2006) 5855–5862.
[6] W.A. Daoud, J.H. Xin, Low temperature sol–gel processed photocatalytic titania coating, J. Sol-Gel Sci. Technol. 29 (2004) 25–29.
[7] B.E. Yoldas, Investigations of porous oxides as an antireflective coating for glass surfaces, Appl. Opt. 19 (1980) 1425–1429.
[8] G.L.T. Nasimento, L.M. Seara, B.R.A. Neves, N.D.S. Mohallem, Textural characterization of porous silica films prepared by the sol–gel process, Progr. Colloid Polym. Sci. 128 (2004) 227–231.
[9] R.K.S. Raman, P.C. Banerjee, D.E. Lobo, H. Gullapalli, M. Sumandasa, A. Kumar, L. Choudhary, R. Tkacz, P.M. Ajayan, M. Majumder, Protecting Cu from electrochemical degradation by graphene coating, Carbon 50 (2012) 4040–4045.
[10] G. Kalita, M.E. Ayhan, S. Sharma, S.M. Shinde, D. Ghimire, K. Wakita, M. Umeno, M. Tanemura, Low temperature deposited graphene by surface wave plasma CVD as effective oxidation resistive barrier, Corros. Sci. 78 (2014) 183–187.
[11] A.S. Kousalya, A. Kumar, R. Paul, D. Zemlyanov, T.S. Fisher, Graphene: an effective oxidation barrier coating for liquid and two-phase cooling systems, Corros. Sci. 69 (2013) 5–10.
[12] N.T. Kirkland, T. Schiller, N. Medhekar, N. Birbilis, Exploring graphene as a corrosion protection barrier, Corros. Sci. 56 (2012) 1–4.
[13] S.S. Chen, L. Brown, M. Levendorf, W.W. Cai, S.Y. Ju, J. Edgeworth, X.S. Li, C.W. Magnuson, A. Velamakanni, R.D. Piner, J.Y. Kang, J. Park, R.S. Ruoff, Oxidation resistance of graphene-coated Cu and Cu/Ni alloy, ACS Nano 5 (2011) 1321–1327.
[14] D. Prasai, J.C. Tuberquia, R.R. Harl, G.K. Jennings, K.I. Bolotin, Graphene: corrosion-inhibiting coating, ACS Nano 6 (2012) 1102–1108.
[15] M. Kalisz, M. Grobelny, M. Mazur, D. Wojcieszak, M. Świniarski, M. Zdrojek, J. Domaradzki, D. Kaczmarek, Mechanical and electrochemical properties of Nb_2O_5, Nb_2O_5:Cu and graphene layers deposited on titanium alloy (Ti6Al4V), Surf. Coat. Technol. 271 (2015) 92–99.
[16] J. Domaradzki, D. Kaczmarek, B. Adamiak, J. Dora, S. Maguda, Polish patent application, P 395 346, 2011.
[17] H.P. Klug, L.E. Alexander, in: H.P. Klug, L.E. Alexander (Eds.), X-ray Diffraction Procedures for Polycrystalline and Amorphous Materials, 2nd ed.John Wiley and Sons, New York, 1974.
[18] X. Liang, B.A. Sperling, I. Calizo, G. Cheng, C.A. Hacker, Q. Zhang, Y. Obeng, K. Yan, H. Peng, Q. Li, X. Zhu, H. Yuan, A.R. Hight Walker, Z. Liu, L. Peng, C.A. Richter, Toward clean and crackless transfer of graphene, ACS Nano 5 (2011) 9144–9153.
[19] A. Jorio, R. Saito, G. Dresselhaus, M.S. Dresselhaus, Raman Spectroscopy in Graphene-Based Systems: Prototypes for Nanoscience and Nanometrology, Wiley-VCH, 2011.
[20] V. Singh, D. Joung, L. Zhai, S. Das, S.I. Khondaker, S. Seal, Graphene based materials: past, present and future, Prog. Mater. Sci. 56 (2011) 1178–1271.
[21] A. Gupta, G. Chen, P. Joshi, S. Tadigadapa, P.C. Eklund, Raman scattering from high-frequency phonons in supported n-graphene layer films, Nano Lett. 6 (2006) 2667–2673.
[22] A.C. Ferrari, J.C. Meyer, V. Scardaci, C. Casiraghi, M. Lazzeri, F. Mauri, S. Piscanec, D. Jiang, K.S. Novoselov, S. Roth, A.K. Geim, Raman spectrum of graphene and graphene layers, Phys. Rev. Lett. 97 (2006) 187401.
[23] W.C. Oliver, G.M. Pharr, An improved technique for determining hardness and elastic modulus using load and displacement sensing indentation experiments, J. Mater. Res. 7 (1992) 1564–1583.
[24] A.C. Fisher-Cripps, Nanoindentation, Springer, New York, 2002.
[25] M. Martyniuk, J. Antoszewski, B.A. Walmsley, C.A. Musca, J.M. Dell, Y.-G. Jung, B.R. Lawn, H. Huang, L. Faraone, Determination of mechanical properties of silicon nitride thin films using nanoindentation, Proc. SPIE 5798 (2005) 216–222.
[26] W. Moćko, M. Szymańska, M. Śmietana, M. Kalisz, Simulation of nanoindentation experiments of single-layer and double-layer thin films using finite element method, Surf. Interface Anal. 46 (2014) 1071–1076.
[27] Y.G. Jung, Evaluation of elastic modulus and hardness of thin films by nanoindentation, J. Mater. Res. 19 (2004) 3076–3080.
[28] W. Lin-Dong, L. Min, L. Nai-Gang, Hardness measurements and evaluation of double-layer films on material surface, Chin. J. Aeronaut. 16 (2003) 212–216.
[29] H. Gao, C.-H. Chiu, J. Lee, Elastic contact versus indentation modeling of multi-layered materials, Int. J. Solids Struct. 29 (1992) 2471–2492.
[30] X.Z. Hu, B.R. Lawn, A simple indentation stress–strain relation for contacts with spheres on bilayer structures, Thin Solid Films 322 (1998) 225.
[31] F. Mansfeld, Electrochemical methods of corrosion testing, ASM International ASM Handbook, 13A 2003, pp. 446–462.
[32] K. Zdunek, K. Nowakowska-Langier, R. Chodun, J. Dora, S. Okrasa, E. Talik, Optimization of gas injection conditions during deposition of AlN layers by novel reactive GIMS method, Mater. Sci. Pol. 32 (2) (2014) 171–175.
[33] G. Boere, Influence of fluoride on titanium in an acidic environment measured by polarization resistance technique, J. Appl. Biomater. 6 (4) (1995) 283–288.
[34] M. Nakagawa, S. Matsuya, T. Shiraishi, M. Ohta, Effect of fluoride concentration and pH on corrosion behavior of titanium for dental use, J. Dent. Res. 78 (1999) 1568–1572.
[35] R.W. Schutz, D.E. Thomas, Corrosion of titanium and titanium alloys, Metals Handbook, 13, American Society for Metals (ASM) International, Metals Park, OH 1987, pp. 669–706.
[36] L. Kinani, A. Chtaini, Corrosion inhibition of titanium in artificial saliva containing fluoride, Leonardo J. Sci. 6 (11) (2007) 33–40.
[37] Y.X. Leng, J.Y. Chen, P. Yang, H. Sun, N. Huang, The microstructure and properties of titanium dioxide films synthesized by unbalanced magnetron sputtering, Nucl. Inst. Methods Phys. Res. B 257 (2007) 451–454.
[38] G. Ramírez, S.E. Rodil, S. Muhl, D. Turcio-Ortega, J.J. Olaya, M. Rivera, E. Camps, L. Escobar- Alarcón, Amorphous niobium oxide thin films, J. Non-Cryst. Solids 356 (50–51) (2010) 2714–2721.
[39] X. Zhou, Graphene oxidation barrier coating, 2011 (Undergraduate Honors Thesis).
[40] Y.Y. Wang, Z.H. Ni, T. Yu, Z.X. Shen, H.M. Wang, Y.H. Wu, W. Chen, A.T.S. Wee, Raman studies of monolayer graphene: the substrate effect, J. Phys. Chem. C 112 (2008) 10637–10640.
[41] L.-C. Chuang, C.-H. Luo, S. Yang, The structure and mechanical properties of thick rutile–TiO_2 films using different coating treatments, Appl. Surf. Sci. 258 (2011) 297–303.
[42] O. Duyar, F. Placido, H.Z. Durusoy, Optimization of TiO_2 films prepared by reactive electron beam evaporation of Ti_3O_5, J. Phys. D Appl. Phys. 41 (2008) 095307.
[43] F. Gao, Theoretical model of intrinsic hardness, Phys. Rev. B 73 (2006) 132104.
[44] Y. Liang, B. Zhang, J. Zhao, Mechanical properties and structural identifications of cubic TiO_2, Phys. Rev. B 77 (2008) 094126.
[45] M.J. Mayo, R.W. Siegel, A. Narayanasamy, W.D. Nix, Mechanical properties of nanophase TiO_2 as determined by nanoindentation, J. Mater. Res. 5 (5) (1990) 1073–1082.
[46] F. Schmidt-Stein, S. Thiemann, S. Berger, R. Hahn, P. Schmuki, Mechanical properties of anatase and semi-metallic TiO_2 nanotubes, Acta Mater. 58 (2010) 6317–6323.
[47] O. Borrero-López, Mark Hoffman, Avi Bendavid, Phil J. Martin, Mechanical properties and scratch resistance of filtered-arc-deposited titanium oxide thin films on glass, Thin Solid Films 519 (2011) 7925.

[48] A. Bendavid, P.J. Martin, H. Takikawa, Deposition and modification of titanium dioxide thin films by filtered arc deposition, Thin Solid Films 360 (2000) 241.
[49] A.R. Bally, P. Hones, R. Sanjines, P.E. Schmid, F. Levy, Mechanical and electrical properties of fcc TiO_{1+x} thin films prepared by r.f. reactive sputtering, Surf. Coat. Technol. 108–109 (1998) 166.
[50] O. Zywitzki, T. Modes, H. Sahm, P. Frach, K. Goedicke, D. Gloß, Structure and properties of crystalline titanium oxide layers deposited by reactive pulse magnetron sputtering, Surf. Coat. Technol. 180–181 (2004) 538.
[51] Y.N. Kok, P.J. Kelly, Properties of pulsed magnetron sputtered TiO_2 coatings grown under different magnetron configurations and power deliver modes, Plasma Process. Polym. 4 (2007) S299.
[52] A. Bendavid, P.J. Martin, E.W. Preston, The effect of pulsed direct current substrate bias on the properties of titanium dioxide thin films deposited by filtered cathodic vacuum arc deposition, Thin Solid Films 517 (2008) 494.
[53] D.S.R. Krishna, Y. Sun, Z. Chen, Magnetron sputtered TiO_2 films on a stainless steel substrate: selective rutile phase formation and its tribological and anti-corrosion performance, Thin Solid Films 519 (2011) 4860.
[54] S.S. Pradhan, S. Sahoo, S.K. Pradhan, Influence of annealing temperature on the structural, mechanical and wetting property of TiO_2 films deposited by RF magnetron sputtering, Thin Solid Films 518 (2010) 6904.